npj | Computational Materials

www.nature.com/npjcompumats

ARTICLE OPEN

High-throughput computational discovery of $In_2Mn_2O_7$ as a high Curie temperature ferromagnetic semiconductor for spintronics

Wei Chen[1], Janine George[1], Joel B. Varley[2], Gian-Marco Rignanese[1] and Geoffroy Hautier[1]

Materials combining strong ferromagnetism and good semiconducting properties are highly desirable for spintronic applications (e.g., in spin-filtering devices). In this work, we conduct a search for concentrated ferromagnetic semiconductors through high-throughput computational screening. Our screening reveals the limited availability of semiconductors combining ferromagnetism and a low effective mass. We identify the manganese pyrochlore oxide $In_2Mn_2O_7$ as especially promising for spin transport as it combines low electron effective mass ($0.29\,m_0$), a large exchange splitting of the conduction band (1.1 eV), stability in air, and a Curie temperature (about 130 K) among the highest of concentrated ferromagnetic semiconductors. We rationalise the high performance of $In_2Mn_2O_7$ by the unique combination of a pyrochlore lattice favouring ferromagnetism with an adequate alignment of O–2*p*, Mn–3*d*, and In–5*s* forming a dispersive conduction band while enhancing the Curie temperature.

npj Computational Materials (2019)5:72 ; https://doi.org/10.1038/s41524-019-0208-x

INTRODUCTION

Materials combining semiconductivity and magnetism open up possibilities for novel electronic devices that utilise electron spin in addition to charge degrees of freedom.[1,2] Ferromagnetic semiconductors (FMSs) are in particular valued for their potential in spintronics for spin-polarised transport. Compared to ferromagnetic metals, FMSs are more suited for injecting spin-polarised electrons into non-magnetic semiconductors.[3–8] A closely related and technologically important phenomenon is spin filtering, which can be realised through the use of FMSs as the tunneling barrier for generating highly spin-polarised current.[9–14]

FMSs used in spintronics are primarily based on magnetic impurities embedded into conventional non-magnetic semiconductors.[15] The robustness of carrier-induced ferromagnetism is extremely sensitive to the growth conditions and processing methods, and the origin of room-temperature ferromagnetism of such diluted magnetic semiconductors remains a subject of debate.[2,16] In contrast, concentrated magnetic semiconductors exhibit long-range magnetism without resorting to extrinsic doping. A few concentrated FMSs have been reported, including Cr halides $CrBr_3$[17,18] and CrI_3,[19–23] Cr spinel selenides,[6] Mn pyrochlore oxides,[24] and perovskites such as $BiMnO_3$,[25] $CuSeO_3$,[26] and $YTiO_3$.[27] Among the most studied FMSs for spintronics are the Eu chalcogenides Eu*X* (*X* = O,S,Se).[10–12,14,28] While providing very good performances in spin-filter devices, the Eu*X* exhibit very low Curie temperature (e.g., $T_C = 69$ K for EuO[29]), which is characteristic for most FMSs known to date.

In addition, the electronic structure of FMSs needs to be tailored in the context of spin transport. For a barrierless electrical spin injection depicted in Fig. 1a, the efficiency is determined by the exchange splitting of the conduction band while a low effective electron mass is appreciated for achieving high carrier mobility. Analogously, the exchange splitting is critical for spin filtering as it gives rise to spin-dependent potential barriers for the tunneling current (cf. Fig. 1b), resulting in spin-polarised current in favour of the spin with a lower potential barrier.[13,30,31] As such, EuO is in particular attractive for spin injection[32] and filtering[12] because of its large exchange splitting of the conduction band (0.6 eV) and highly dispersive conduction band.[33] Nevertheless, its poor air stability[34–37] along with the low T_C present major obstacles for practical applications.

Combining strong ferromagnetism and attractive semiconducting properties in one material is therefore desirable but remains an open problem. Here, we set out to identify systematically concentrated FMSs through a large-scale computational screening of known compounds. We report on the materials identified and especially their semiconducting properties, their Curie–Weiss temperatures, and their stabilities. In particular, we identify the Mn pyrochlore oxide $In_2Mn_2O_7$ as a very promising material. We discuss its potential use for spin transport and the inherent structural and chemical reasons for its high performances.

RESULTS

We consider a material to be a good FMS candidate if it offers a high ferromagnetic transition temperature and good semiconducting properties. Because electrons have much longer spin lifetimes than holes,[2] we focus on spin transport based on electrons as illustrated in Fig. 1, and hence look for FMSs with a large exchange splitting of the conduction band and a low electron effective mass. Starting from the materials project (MP) database comprising over 40,000 density-functional theory (DFT) calculations using the semilocal Perdew–Burke–Ernzerhof (PBE) functional[38] and the Hubbard *U* correction (PBE + *U*)[39] (for

[1]Institute of Condensed Matter and Nanoscience (IMCN), Université catholique de Louvain, 1348 Louvain-la-Neuve, Belgium and [2]Lawrence Livermore National Laboratory, Livermore, CA 94550, USA
Correspondence: Geoffroy Hautier (geoffroy.hautier@uclouvain.be)

Received: 26 February 2019 Accepted: 20 June 2019
Published online: 11 July 2019

transition-metal oxides), we first screen the materials based on their thermodynamic stability (energy above convex hull at 0 K lower than 50 meV per atom) and electronic band gap (>100 meV). This step leads to about 15,300 semiconductors, out of which 3100 compounds show a finite magnetic moment (>0.5 μ_B) in the ground state (when the computation is initialised in a ferromagnetic state). Among these magnetic materials, only about 1000 compounds exhibit an electron effective mass (m_e^*) smaller than 1.5 m_0. In comparison, typical semiconductors (e.g. GaAs, Si, and ZnO) present m_e^* ranging from 0.05 to 0.5 m_0.[40] Figure 2a shows the distribution of m_e^* for materials exhibiting a finite magnetisation compared to non-magnetic materials. It is clear that low m_e^* is more easily achieved in non-magnetic compounds. The need for magnetism often implies partially filled *d* bands. When the conduction-band character is dominated by these orbitals, their localised nature leads to a high effective mass.[41] Figure 2b confirms that low m_e^* materials are mainly of *s* character. The poor effective mass and strong ferromagnetism are, for instance, present in $CrBr_3$ and certain manganites such as $LaMnO_3$, where a predominant 3*d* character in the lowest conduction band leads to a high m_e^* of over 10 m_0. At variance, the low m_e^* of EuO (0.4 m_0) is remarkable in that the ferromagnetism arises from an indirect exchange between the localised Eu–4*f* electrons in the valence and the delocalised 5*d*/6*s* electrons in the conduction band.[33,42]

The presence of a non-zero total magnetisation in the 0 K DFT computation with an initial ferromagnetic ordering does not imply that the ground state is necessarily ferromagnetic and that this ferromagnetic configuration is sustained at high temperature. We thereby estimate the magnetic ordering of the ~1000 compounds by comparing the total energies of the ferromagnetic ground state to the antiferromagnetic (AFM) or ferrimagnetic (FiM) one. The difference serves as an indicator of whether the compound in question is dominated by ferromagnetic exchange interactions. To determine the magnetic ground state, we use supercells that contain at least four atoms for each distinct magnetic species. An exhaustive search of the lowest-energy AFM (or FiM) configuration is carried out by enumerating all possible configurations in which half of the magnetic sites are initialised with a positive magnetic moment whereas the other half with a negative magnetic moment. The absolute value of the initial magnetic moment follows the calculated magnetic moment in the FM configuration. We consider only the collinear magnetic configurations as non-collinear calculations would be computationally prohibitive at this stage of screening. We find that less than 30 compounds favour an FM ground state by over 10 meV per formula unit compared to the AFM or FiM configurations (see Table S1 of Supplementary Information), manifesting already the difficulty of finding semiconductors with robust ferromagnetism.

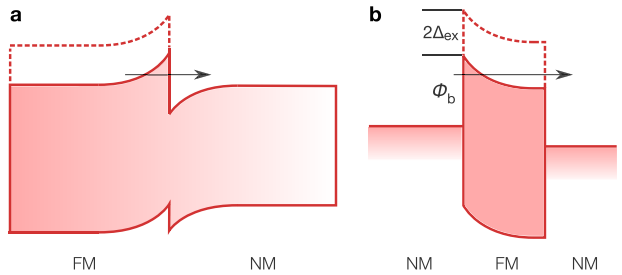

Fig. 1 Band diagram schematics of spin-polarised electron injection using a ferromagnetic (FM)/non-magnetic (NM) *n*–*n* heterojunction **a** and of spin filtering achieved with an FM tunneling barrier sandwiched between two NM metal contacts **b**. For the ferromagnetic semiconductor, the exchange splitting of the conduction band amounts to $2\Delta_{ex}$ and is depicted by dashed lines

Our computational screening thus far relies on the PBE(+ *U*) calculations. While instrumental in determining the energetic stability among various magnetic orderings, PBE and PBE + *U* with *U* values calibrated for formation enthalpies do not warrant a faithful description of the underlying electronic structure. For a higher accuracy and a better treatment, particularly of localised *d* and *f* electrons, hybrid functionals such as the Heyd–Scuseria–Ernzerhof (HSE) functional[43,44] should be used.[45] We have thus performed HSE calculations on the candidates exhibiting the most favourable ferromagnetic ordering (The HSE calculations exclude the pyrochlore oxides containing the lanthanide elements with partially filled *f* electrons due to convergence issues. Nevertheless, these materials are expected to exhibit more exotic magnetic properties than the simple ferromagnetic ordering[24]). We report in Table 1 the electron effective mass as well as the Curie–Weiss temperature θ_{CW} obtained from HSE calculations. The latter is defined from the paramagnetic response at high temperature, and is estimated with the random-phase approximation[46] as described in Supplementary Information. When known, we also report on their experimental Curie temperature T_C. The difference between θ_{CW} and T_C indicates the degree of geometrical frustration in a magnetic system.[24] Notably, the FMSs listed in Table 1 can be classified into five categories: Eu chalcogenides, Cr spinel

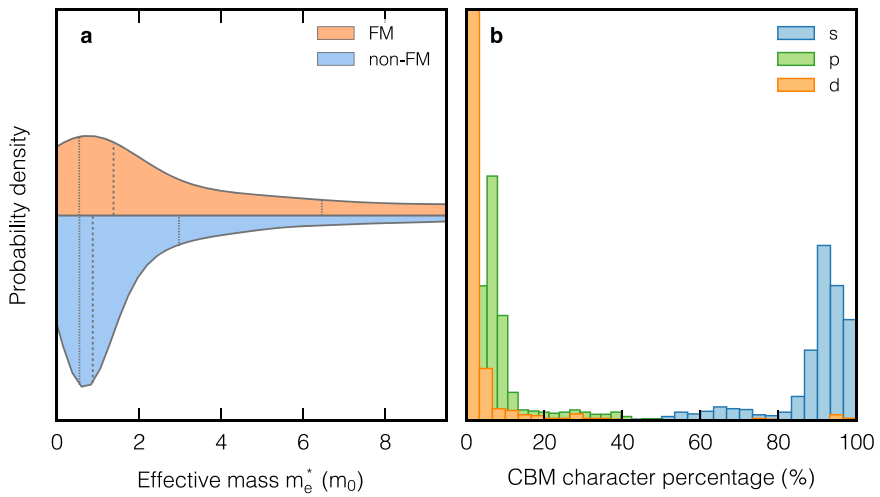

Fig. 2 **a** Violin plot of electron effective masses for semiconductors in the FM and non-FM configurations. The vertical lines refer to the median value along with the first and third quartiles. **b** Probability distribution of the orbital characters in the conduction band minimum for FM semiconductors with an electron effective mass smaller than 1.5 m_0

Table 1. Properties of identified ferromagnetic semiconductors evaluated with HSE hybrid functional, including the exchange splitting of the conduction band ($2\Delta_{ex}$), electron effective mass (m_e), and Curie–Weiss temperature (θ_{CW})

	$2\Delta_{ex}$ (eV)	m_e (m_0)	θ_{CW} (K)	θ_{CW}^{expt} (K)	T_C^{expt} (K)
Eu chalcogenides					
EuO	1.04	0.38	101	76[a]	69[a]
EuS	0.60	0.44	30	19[a]	16.5[a]
EuSe	0.54	0.44	19	9[a]	7[a]
Cr spinels					
$CdCr_2S_4$	0.11	0.29	202	152[b]	84.5[c]
$CdCr_2Se_4$	0.21	0.51	237	204[b]	129.5[c]
$MgCr_2S_4$	0.46	0.70	170		
$MgCr_2Se_4$	0.78	0.60	216		
$HgCr_2S_4$	0.83	0.15	209	142[d]	36.0[d]
$HgCr_2Se_4$	0.54	0.12	241	200[d]	106[d]
$ZnCr_2S_4$	0.48	0.32	134	7.9[e]	
$ZnCr_2Se_4$	0.11	0.23	186	90[e]	
Mn(V)-pyrochlores					
$In_2Mn_2O_7$	0.62	0.29	133	155[f]	129[f]
$Sc_2Mn_2O_7$	1.05	0.80	68	77[g]	20[g]
$Y_2Mn_2O_7$	1.38	0.81	63	50[f]	16[f]
$Lu_2Mn_2O_7$	1.29	0.81	68	60[f]	15[f]
$Lu_2V_2O_7$	0.87	0.62	40	97[h]	74[h]
$Y_2V_2O_7$	0.87	0.62	41		
Bi manganites					
$BiMnO_3$	1.25	0.60	160	120[i]	105[i]
Double perovskites					
La_2NiMnO_6	1.33	1.12	268	302[j]	270–280[k]
La_2CoMnO_6	1.13	1.37	264	300[l]	226[l]
Bi_2NiMnO_6	1.51	0.70	174	140[m]	140[m]
Bi_2CoMnO_6	1.39	0.69	116		95[n]

The experimental Curie–Weiss and Curie temperature are given if available
[a]ref. [29]
[b]ref. [87]
[c]ref. [88]
[d]ref. [48]
[e]ref. [89]
[f]ref. [61]
[g]ref. [90]
[h]ref. [91]
[i]ref. [92]
[j]ref. [93]
[k]refs. [47,93]
[l]ref. [94]
[m]ref. [95]
[n]ref. [96]

chalcogenides, Bi manganites, Mn pyrochlore oxides, and Mn double perovskites. Figure 3 shows the HSE band structure for a representative compound in each category. Our screening recovers the well-known FMSs in the context of spintronics such as EuO, $CdCr_2Se_4$, and $BiMnO_3$. Less traditionally associated to spintronics are the Mn pyrochlores (e.g., $In_2Mn_2O_7$).

To compare the performances of these different compounds, we plot in Fig. 4 m_e^* vs θ_{CW} obtained from HSE calculations. We further indicate the stability of the materials against oxidation by showing the maximum oxygen chemical potential reachable while keeping the material thermodynamically stable. This provides a measure of air sensitivity: the higher oxygen chemical potential, the greater stability. The highest θ_{CW} is clearly obtained among the double perovskites $LaBMnO_6$ (B = Ni, Co). In particular, La_2NiMnO_6 shows near room-temperature ferromagnetism arising from the strong ferromagnetic superexchange interactions between the Mn^{4+} and Ni^{2+}.[47] However, the large m_e^* of over 1.1 m_0 could be a limiting factor for high mobility applications. Following La_2NiMnO_6, the sulfide and selenide spinels ACr_2X_4 (A = Hg, Cd, Zn, and Mg; X = S, Se) show θ_{CW} up to 200 K. The prevalence of Cr^{3+} can be related to the high magnetic moment of its d^3 configuration. The strongest ferromagnetism is observed in $CdCr_2Se_4$ in accordance with experiment.[48] $MgCr_2Se_4$, which has been overlooked as a ferromagnetic spinel in literature, shows comparable ferromagnetism as $CdCr_2Se_4$ according to our computational screening. In any case, all these spinel chalcogenides show poor stability in air due to their sulfide or selenide chemistry. The air stability is also an issue for Eu chalcogenides. In fact, EuO is known for the difficulty in growing high-quality thin films since Eu^{2+} is easily oxidised to Eu^{3+}.[34–37] The remaining oxides are the pyrochlores and $BiMnO_3$. Among the pyrochlores, $In_2Mn_2O_7$ is especially noteworthy as it shows the highest θ_{CW} and the lowest m_e^*. While showing similar electronic and magnetic properties as $BiMnO_3$, $In_2Mn_2O_7$ exhibits a higher air stability thanks to their high stability of the oxidation states of its cations: In^{3+} and Mn^{4+}. In comparison with EuO, it offers an even lower m_e^* (0.29 m_0), better air stability, and a significantly higher θ_{CW} (155 K vs 76 K).

The calculated exchange splitting of the conduction band shown in Table 1 for the candidates confirms the good performance in spin filtering with EuO[12] and $BiMnO_3$.[25] Table 1 implies that $In_2Mn_2O_7$ should also present an excellent spin-filter effect. But as uncertainty remains in the exchange splitting with the HSE calculations and little is known from experiment, we resort to the self-consistent quasiparticle *GW* calculations (QS*GW*) with vertex corrections[49] to calculate the electronic structure of $In_2Mn_2O_7$. The QS*GW* method does not depend on any adjustable parameter and starting point, and it has been shown to provide a reasonable description of the electronic structure for correlated transition-metal oxides.[50] As shown in the QS*GW* band structure in Fig. 5a, the exchange splitting further opens up to 1.1 eV, in support of using $In_2Mn_2O_7$ for efficient spin filtering.

DISCUSSION

Our large-scale computational screening shows that the viable routes toward ferromagnetism in semiconducting materials involve either the partially filled Eu–4*f* electrons or the partially filled 3*d* electrons of transition metals such as Cr, Mn, and to some extent, V. Indeed, the identified FMSs are mostly Cr spinels and Mn pyrochlores. They are commonly characterised by the high-spin $S = 3/2$ state in the $3d^3$ configuration, which in the (pseudo)cubic crystal field results in an occupied t_{2g} and an unoccupied e_g manifold of states. For Cr spinels, the strength of ferromagnetism reduces from selenides to sulfides, and eventually inverts to antiferromagnetism for oxides as the ferromagnetic t_{2g}–e_g exchange interaction is outweighed by the AFM t_{2g}–t_{2g} interaction.[51] While the same competing mechanism is also at play for the pyrochlores, the larger lattice constant stabilises the ferromagnetic configuration for a series of Mn and V pyrochlore oxides. The double perovskites, on the other hand, offer significantly higher T_C than the simple perovskite counterparts such as $BiMnO_3$ and $LaMnO_3$. The anomalously strong ferromagnetism of La_2NiMnO_6 stems from the fully occupied e_g state of Ni^{2+}, which is unique to this type of material. In comparison, the e_g state is either partially occupied for the Mn^{3+} in $BiMnO_3$, or simply empty for the Mn^{4+} and Cr^{3+} in the case of pyrochlores and spinels.

Our results confirm the challenge in combining adequate air stability, effective mass, and Curie temperature. $In_2Mn_2O_7$ offers an exceptional compromise between these three metrics. Among

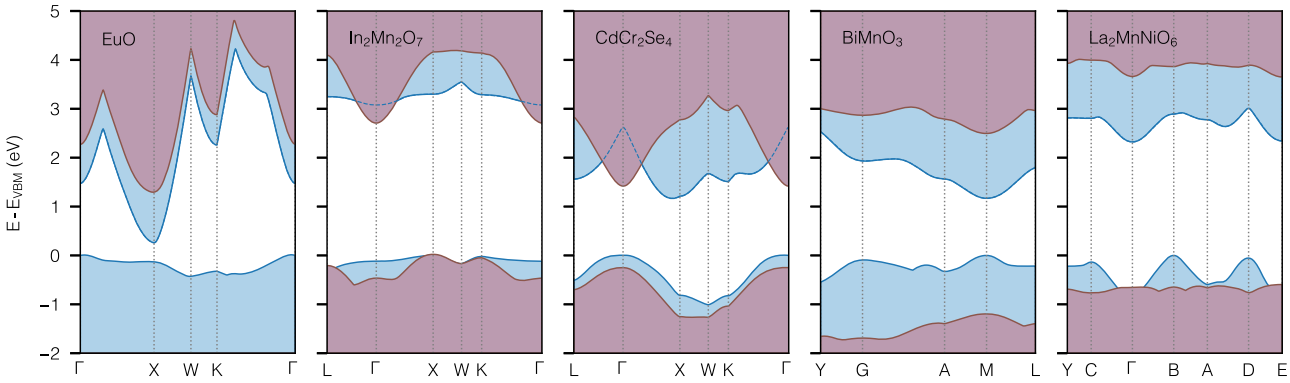

Fig. 3 Spin-polarised band structures of the five representative ferromagnetic semiconductors obtained with HSE hybrid-functional calculations. The majority and minority spin channels are shaded by the blue and light red colours, respectively

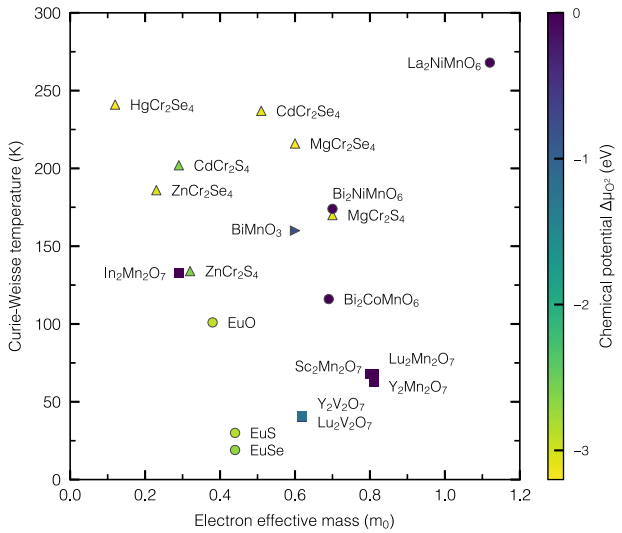

Fig. 4 Figure of merit of the ferromagnetic semiconductors identified through the computational screening. $\Delta\mu_{O_2}$ indicates the oxygen chemical potential (referred to the isolated molecule) below which the compound is stable in an oxidising atmosphere. Oxidisation is more likely for compounds with a more negative $\Delta\mu_{O_2}$

the ferromagnetic pyrochlore materials, $In_2Mn_2O_7$ shows a very low m_e^* of 0.29 m_0, which is among the lowest for all identified FMSs. Such a low effective mass is the result of the prominent In–5*s* character of the conduction band minimum (CBM) in the minority spin channel, as clearly shown by the element-resolved band structure in Fig. 5a. In contrast, most pyrochlore oxides, such as $Y_2Mn_2O_7$, exhibit much less dispersive CBM in both spin channels (cf. Fig. 5b) as the Y–5*s* states do not mix in the lower conduction band. In–5*s* states are known to lead to dispersive conduction band in binary and ternary oxides:[41] one of the highest electron mobility oxide being doped In_2O_3.

The *s* character in the conduction band is also at the origin of the strong ferromagnetism present in $In_2Mn_2O_7$, leading to the highest T_C among all pyrochlore oxides. Apparently, the semi-empirical Goodenough–Kanamori rules of superexchange[52,53] do not fully account for such strong ferromagnetism as all the pyrochlore oxides considered in Table 1 show Mn–O–Mn bond angles between 130° and 133°. Longer Mn–O bond lengths reduce the AFM t_{2g}–t_{2g} interactions among neighbouring Mn atoms, yet this does not explain the higher T_C of $In_2Mn_2O_7$ ($d_{Mn-O} = 1.89$ Å) compared to $Y_2Mn_2O_7$ ($d_{Mn-O} = 1.91$ Å). Indeed, the hybridisation among Mn(t_{2g})–O(*p*)–In(*s*) states is key to the strong ferromagnetism of $In_2Mn_2O_7$. Specifically, the In–O covalency mixes with the Mn-t_{2g}–O-*p* states, stabilising the ferromagnetic configuration by shifting the In–O states upward (downward) in the majority (minority) channel.[54] This is supported by the band-resolved crystal orbital Hamilton population (COHP) analysis,[55–59] showing the antibonding nature of In(5*s*)–O and Mn–O interactions at the CBM of the minority spin channel (see Table S2 and Fig. S2 of Supplementary Information). More intuitively, the enhanced ferromagnetism can be understood by the indirect-exchange mechanism[60] involving virtual electron hopping from the O–*p* to the In–*s* states in the conduction band. This leaves the O–*p* state effectively spin polarised and enhances the ferromagnetic super-exchange through the O atom. For this mechanism to take effect, the atomic valence *s* state needs to be in a reasonable proximity to the O–*p* state, which is exactly the case of the group 13 elements such as In and Tl, although $Tl_2Mn_2O_7$ is a half-metal.[54,60–63] While pyrochlore oxides comprising other group 13 elements (such as B, Al, and Ga) do not appear as a candidate because of their instability, they indeed exhibit a highly dispersive *s*-like CBM from the minority channel and a high θ_{CW} comparable to $In_2Mn_2O_7$ (see Table S3 of Supplementary Information for the properties of these hypothetical pyrochlore oxides).

Finally, the FMSs need to be *n*-type to facilitate the transport of spin-polarised electrons. To this end, we assess several dopants in $In_2Mn_2O_7$, among which Sn and Mo are found to incorporate on the In site while acting as shallow donors, analogous to that in In_2O_3.[64,65] The computational details of defect calculations are described in Supplementary Information, whereas the formation energies of the dopants in various charge states are given in Fig. S1. We additionally find no evidence of favourable self-trapping of electrons as small polarons in this material and a general unfavourability of native compensating centers like cation vacancies, which suggests that $In_2Mn_2O_7$ can be effectively *n*-type doped.

In conclusion, we have carried out a large-scale computational screening in quest of concentrated FMSs. Among the very few identified materials, the pyrochlore oxide $In_2Mn_2O_7$ emerges as a particularly interesting candidate that exhibits robust ferromagnetism, good air stability, and a low electron effective mass, an uncommon combination that is of great promise for high mobility spin transport. While $In_2Mn_2O_7$ does not yet fulfill the requirement of room-temperature ferromagnetism, its Curie temperature could be potentially increased with epitaxial strain.[66–68] Indeed, as shown in Supplementary Information, we find that tensile stress due to the lattice mismatch to some semiconductor substrates (such as Si and GaAs) can effectively increase the Curie temperature of $In_2Mn_2O_7$, but it needs to be practiced with caution as it has adverse effects on the effective mass (see Fig. S3). Other routes, such as doping, can also be explored to enhance the

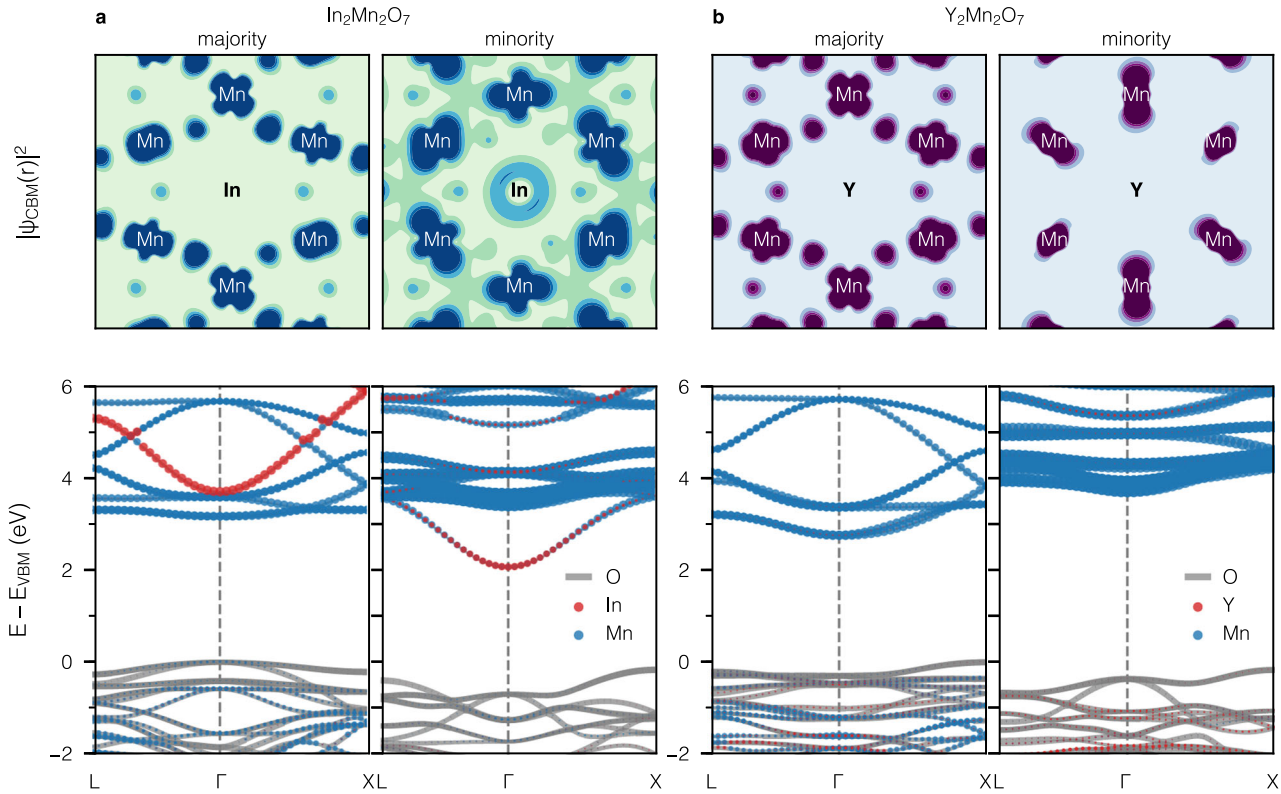

Fig. 5 Electron density distributions of the lowest conduction band at the Γ point and QS*GW* band structures for $In_2Mn_2O_7$ **a** and $Y_2Mn_2O_7$ **b** in the ferromagnetic configuration. The electron density is plotted on the (111) plane centered at an In (Y) atom, whereas the characters associated with the states are resolved by the fat bands mapped onto the atoms. The significant *s* character in the lowest conduction band of $In_2Mn_2O_7$ is absent in $Y_2Mn_2O_7$

Curie temperature as it has been demonstrated for EuO and $BiMnO_3$.[68–72]

METHODS

First-principles calculations

Collinear spin-polarised semilocal DFT–PBE and hybrid functional HSE calculations are performed with the Vienna ab initio simulation package (VASP).[73,74] Electron–ion interactions are described by the projector-augmented-wave (PAW) method.[75,76] We use the Pymatgen package[77] to generate VASP input files based on the structures retrieved from the MP database. Throughout the calculations, the kinetic energy cut-off is set to 520 eV, and a regular Γ-centered **k**-point mesh is used with a grid density of 1600 **k** points per atom. For transition-metal oxides, the PBE calculation is carried out with the Hubbard *U* correction (PBE + *U*), for which the *U* parameters take the values adopted by the MP following the approach described by Wang et al.[78]

Quasiparticle self-consistent *GW* calculations are performed with the ABINIT code[79,80] using the PseudoDojo optimised norm-conserving pseudopotentials.[81,82] Vertex corrections in the dielectric screening are accounted for through the use of the bootstrap exchange-correlation kernel.[49,83] The dielectric function is evaluated through the contour deformation method[84] including unoccupied states up to 150 eV above the Fermi level in the summations. The dielectric matrix is represented by a plane-wave basis set with an energy cut-off of 160 eV. The self-consistent iteration of the wavefunctions is restricted to the lowest $2N_v$ states where N_v is the number of the valence bands.

Band-resolved COHP calculations are carried out with a development version of the LOBSTER package.[55–59] The pbeVaspFit2015 basis is used with the following basis functions: O: 2*s*, 2*p*; In: 5*s*, 5*p*, and 4*d*; Mn: 4*s*, 3*p*, and 3*d*. The wavefunctions are obtained using the PBE + *U* functional.

Effective mass calculation

The reported effective mass is defined as the conductivity effective mass

$$(m^*)^{-1} = \frac{\sigma(T,\mu)}{n(T,\mu)e^2\tau}, \quad (1)$$

where the electrical conductivity σ and the charge carrier concentration n are computed directly from the Boltztrap calculations[85] with $T = 300$ K and a chemical potential μ leading to $n = 10^{18}$ cm^{-3}. The relaxation time τ is assumed to be independent of T and μ following previous high-throughput works.[41,86]

DATA AVAILABILITY

All data generated or analysed during this study are included in this published article (and its Supplementary Information files).

ACKNOWLEDGEMENTS

G.-M.R. acknowledges the F.R.S.-FNRS for funding. G.H., G.-M.R. and J.G. acknowledge the F.R.S.-FNRS project HTBaSE (Contract no. PDR-T.1071.15) for financial support. W. C. and G.-M.R. acknowledge support from the Communauté française de Belgique through the BATTAB project (Project no. RC 14/19-057). The work by J.B.V. has been performed under the auspices of the U.S. Department of Energy by Lawrence Livermore National Laboratory under Contract no. DE-AC52-07NA27344. Computational resources have been provided by the supercomputing facilities of the Université catholique de Louvain (CISM/UCL) and the Consortium des Equipements de Calcul Intensif en Fédération Wallonie Bruxelles (CECI) funded by the Fonds de la Recherche Scientifique de Belgique (F.R.S.-FNRS) under Grant no. 2.5020.11. The present research has also benefited from computational resources made available on the Tier-1 supercomputer of the Fédération Wallonie-Bruxelles, infrastructure funded by the Walloon Region under Grant no. 1117545. We thank Darrel Schlom for useful discussions, and Richard Dronskowski and Ryky Nelson for a development version of Lobster. The MP is funded by the U.S. Department of Energy, Office of Science, Office of Basic Energy Science, Materials Sciences and Engineering Division under Contract no. DE-AC02-05-CH11231: Materials Project program KC23MP.

AUTHOR CONTRIBUTIONS

G.H. and W.C. conceived the study. W.C. carried out the high-throughput computational screening and calculated the electronic and magnetic properties of the compounds. J.G. did the COHP analysis and J.B.V. performed the defect calculation for $In_2Mn_2O_7$. All authors analysed the results. The manuscript is written by W.C. with inputs from J.G. and J.B.V. and is approved by all authors.

ADDITIONAL INFORMATION

Supplementary information accompanies the paper on the *npj Computational Materials* website (https://doi.org/10.1038/s41524-019-0208-x).

Competing interests: The authors declare no competing interests.

Publisher's note: Springer Nature remains neutral with regard to jurisdictional claims in published maps and institutional affiliations.

REFERENCES

1. Prinz, G. A. Magnetoelectronics. *Science.* **282**, 1660 (1998).
2. Žutić, I., Fabian, J. & Das Sarma, S. Spintronics: fundamentals and applications. *Rev. Mod. Phys.* **76**, 323 (2004).
3. Ohno, Y. et al. Electrical spin injection in a ferromagnetic semiconductor heterostructure. *Nature.* **402**, 790 (1999).
4. Schmidt, G., Ferrand, D., Molenkamp, L. W., Filip, A. T. & van Wees, B. J. Fundamental obstacle for electrical spin injection from a ferromagnetic metal into a diffusive semiconductor. *Phys. Rev. B.* **62**, R4790 (2000).
5. Zhao, H. B. et al. Band offsets at $CdCr_2Se_4$–(AlGa)As and $CdCr_2Se_4$–ZnSe interfaces. *Appl. Phys. Lett.* **82**, 1422 (2003).
6. Kioseoglou, G. et al. Electrical spin injection from an n-type ferromagnetic semiconductor into a III–V device heterostructure. *Nat. Mater.* **3**, 799 (2004).
7. Toyosaki, H., Fukumura, T., Ueno, K., Nakano, M. & Kawasaki, M. A ferromagnetic oxide semiconductor as spin injection electrode in magnetic tunnel junction. *Jpn. J. Appl. Phys.* **44**, L896 (2005).
8. Felser, C., Fecher, G. H. & Balke, B. Spintronics: a challenge for materials science and solid-state chemistry. *Angew. Chem. Int. Ed.* **46**, 668 (2007).
9. Esaki, L., Stiles, P. J. & Molnar, Sv Magnetointernal field emission in junctions of magnetic insulators. *Phys. Rev. Lett.* **19**, 852 (1967).
10. Moodera, J. S., Hao, X., Gibson, G. A. & Meservey, R. Electron-spin polarization in tunnel junctions in zero applied field with ferromagnetic EuS barriers. *Phys. Rev. Lett.* **61**, 637 (1988).
11. Moodera, J. S., Meservey, R. & Hao, X. Variation of the electron-spin polarization in EuSe tunnel junctions from zero to near 100% in a magnetic field. *Phys. Rev. Lett.* **70**, 853 (1993).
12. Santos, T. S. & Moodera, J. S. Observation of spin filtering with a ferromagnetic *EuO* tunnel barrier. *Phys. Rev. B.* **69**, 241203 (2004).
13. Moodera, J. S., Santos, T. S. & Nagahama, T. The phenomena of spin-filter tunnelling. *J. Phys. Condens. Matter.* **19**, 165202 (2007).
14. Santos, T. S. et al. Determining exchange splitting in a magnetic semiconductor by spin-filter tunneling. *Phys. Rev. Lett.* **101**, 147201 (2008).
15. Sato, K. et al. First-principles theory of dilute magnetic semiconductors. *Rev. Mod. Phys.* **82**, 1633 (2010).
16. Dietl, T. A ten-year perspective on dilute magnetic semiconductors and oxides. *Nat. Mater.* **9**, 965 (2010).
17. Tsubokawa, I. On the magnetic properties of a $CrBr_3$ single crystal. *J. Phys. Soc. Jpn.* **15**, 1664 (1960).
18. Ghazaryan, D. et al. Magnon-assisted tunnelling in van der waals heterostructures based on $CrBr_3$. *Nat. Electron.* **1**, 344 (2018).
19. Dillon, J. F. & Olson, C. E. Magnetization, resonance, and optical properties of the ferromagnet CrI_3. *J. Appl. Phys.* **36**, 1259 (1965).
20. McGuire, M. A., Dixit, H., Cooper, V. R. & Sales, B. C. Coupling of crystal structure and magnetism in the layered, ferromagnetic insulator CrI_3. *Chem. Mater.* **27**, 612 (2015).
21. Huang, B. et al. Layer-dependent ferromagnetism in a van der waals crystal down to the monolayer limit. *Nature.* **546**, 270 (2017).
22. Zhong, D. et al. Van der waals engineering of ferromagnetic semiconductor heterostructures for spin and valleytronics. *Sci. Adv.* **3**, e1603113 (2017).
23. Wang, Z. et al. Very large tunneling magnetoresistance in layered magnetic semiconductor CrI_3. *Nat. Commun.* **9**, 2516 (2018).
24. Gardner, J. S., Gingras, M. J. P. & Greedan, J. E. Magnetic pyrochlore oxides. *Rev. Mod. Phys.* **82**, 53 (2010).
25. Gajek, M. et al. Spin filtering through ferromagnetic $BiMnO_3$ tunnel barriers. *Phys. Rev. B.* **72**, 020406 (2005).
26. Kohn, K., Inoue, K., Horie, O. & Akimoto, S.-I. Crystal chemistry of $MSeO_3$ and $MTeO_3$ (M = Mg, Mn, Co, Ni, Cu, and Zn). *J. Solid State Chem.* **18**, 27 (1976).
27. Garrett, J., Greedan, J. & MacLean, D. A. Crystal growth and magnetic anisotropy of $YTiO_3$. *Mater. Res. Bull.* **16**, 145 (1981).
28. Wachter, P. Europium chalcogenides: EuO, EuS, EuSe and EuTe. In *Handbook on the Physics and Chemistry of Rare Earths*, Vol. 2: Alloys and Intermetallics, Ch. 19, 507–574 (Elsevier, Amsterdam, Netherlands, 1979).
29. McGuire, T. R. & Shafer, M. W. Ferromagnetic europium compounds. *J. Appl. Phys.* **35**, 984 (1964).
30. Santos, T. S. *Europium Oxide as a Perfect Electron Spin Filter.* Ph.D. thesis, Massachusetts Inst. Tech. (2007).
31. Bibes, M. & Barthelemy, A. Oxide spintronics. *IEEE Trans. Electron Devices.* **54**, 1003 (2007).
32. Averyanov, D. V. et al. Direct epitaxial integration of the ferromagnetic semiconductor EuO with silicon for spintronic applications. *ACS Appl Mater. Interfaces.* **7**, 6146 (2015).
33. Steeneken, P. G. et al. Exchange splitting and charge carrier spin polarization inEuO. *Phys. Rev. Lett.* **88**, 047201 (2002).
34. Shafer, M., Torrance, J. & Penney, T. Relationship of crystal growth parameters to the stoichiometry of EuO as determined by i.r. and conductivity measurements. *J. Phys. Chem. Solids.* **33**, 2251 (1972).
35. Lettieri, J. et al. Epitaxial growth and magnetic properties of EuO on (001)Si by molecular-beam epitaxy. *Appl. Phys. Lett.* **83**, 975 (2003).
36. Schmehl, A. et al. Epitaxial integration of the highly spin-polarized ferromagnetic semiconductor EuO with silicon and GaN. *Nat. Mater.* **6**, 882 (2007).
37. Mairoser, T. et al. High-quality EuO thin films the easy way via topotactic transformation. *Nat. Commun.* **6**, 7716 (2015).
38. Perdew, J. P., Burke, K. & Ernzerhof, M. Generalized gradient approximation made simple. *Phys. Rev. Lett.* **77**, 3865 (1996).
39. Dudarev, S. L., Botton, G. A., Savrasov, S. Y., Humphreys, C. J. & Sutton, A. P. Electron-energy-loss spectra and the structural stability of nickel oxide: an lsda+u study. *Phys. Rev. B.* **57**, 1505 (1998).
40. Ricci, F. et al. An ab initio electronic transport database for inorganic materials. *Sci. Data.* **4**, 170085 (2017).
41. Hautier, G., Miglio, A., Waroquiers, D., Rignanese, G.-M. & Gonze, X. How does chemistry influence electron effective mass in oxides? A high-throughput computational analysis. *Chem. Mater.* **26**, 5447 (2014).
42. Schlipf, M., Betzinger, M., Ležaić, M., Friedrich, C. & Blügel, S. Structural, electronic, and magnetic properties of the europium chalcogenides: a hybrid-functional DFT study. *Phys. Rev. B* **88**, 094433 (2013).
43. Heyd, J., Scuseria, G. E. & Ernzerhof, M. Hybrid functionals based on a screened coulomb potential. *J. Chem. Phys.* **118**, 8207 (2003).
44. Heyd, J., Scuseria, G. E. & Ernzerhof, M. Erratum: "hybrid functionals based on a screened coulomb potential". *J. Chem. Phys.* **124**, 219906 (2006).
45. Stroppa, A., Kresse, G. & Continenza, A. Revisiting Mn-doped Ge using the Heyd–Scuseria–Ernzerhof hybrid functional. *Phys. Rev. B.* **83**, 085201 (2011).
46. Pajda, M., Kudrnovský, J., Turek, I., Drchal, V. & Bruno, P. Ab initio calculations of exchange interactions, spin-wave stiffness constants, and Curie temperatures of Fe,Co, and Ni. *Phys. Rev. B.* **64**, 174402 (2001).
47. Rogado, N. S., Li, J., Sleight, A. W. & Subramanian, M. A. Magnetocapacitance and magnetoresistance near room temperature in a ferromagnetic semiconductor: La_2NiMnO_6. *Adv. Mater.* **17**, 2225 (2005).
48. Baltzer, P. K., Wojtowicz, P. J., Robbins, M. & Lopatin, E. Exchange interactions in ferromagnetic chromium chalcogenide spinels. *Phys. Rev.* **151**, 367 (1966).
49. Chen, W. & Pasquarello, A. Accurate band gaps of extended systems via efficient vertex corrections in *GW*. *Phys. Rev. B* **92**, 041115 (2015).
50. Faleev, S. V., van Schilfgaarde, M. & Kotani, T. All-electron self-consistent *gw* approximation: application to si, mno, and nio. *Phys. Rev. Lett.* **93**, 126406 (2004).
51. Yaresko, A. N. Electronic band structure and exchange coupling constants in ACr_2X_4 spinels (A = Zn, Cd, Hg; X = O, S, Se). *Phys. Rev. B.* **77**, 115106 (2008).
52. Goodenough, J. B. Theory of the role of covalence in the perovskite-type manganites [La,*M*(II)]MnO_3. *Phys. Rev.* **100**, 564 (1955).
53. Kanamori, J. Superexchange interaction and symmetry properties of electron orbitals. *J. Phys. Chem. Solids.* **10**, 87 (1959).
54. Saha-Dasgupta, T., De Raychaudhury, M. & Sarma, D. D. Origin of ferromagnetism and its pressure and doping dependence in $Tl_2Mn_2O_7$. *Phys. Rev. Lett.* **96**, 087205 (2006).
55. Dronskowski, R. & Blöchl, P. E. Crystal orbital Hamilton populations (COHP): energy-resolved visualization of chemical bonding in solids based on density-functional calculations. *J. Phys. Chem.* **97**, 8617 (1993).
56. Deringer, V. L., Tchougréeff, A. L. & Dronskowski, R. Crystal orbital hamilton population (COHP) analysis as projected from plane-wave basis sets. *J. Phys. Chem. A.* **115**, 5461 (2011).

57. Maintz, S., Deringer, V. L., Tchougréeff, A. L. & Dronskowski, R. Analytic projection from plane-wave and PAW wavefunctions and application to chemical-bonding analysis in solids. *J. Comput. Chem.* **34**, 2557 (2013).
58. Maintz, S., Deringer, V. L., Tchougréeff, A. L. & Dronskowski, R. LOBSTER: A tool to extract chemical bonding from plane-wave based DFT. *J. Comput. Chem.* **37**, 1030 (2016).
59. Sun, X. et al. Achieving band convergence by tuning the bonding ionicity in n-type Mg_3Sb_2. *J. Comput. Chem.* **40**, 1693 (2019).
60. Mishra, S. K. & Satpathy, S. Electronic structure and exchange interactions in the manganese-based pyrochlore oxides. *Phys. Rev. B.* **58**, 7585 (1998).
61. Shimakawa, Y. et al. Crystal structure, magnetic and transport properties, and electronic band structure of $A_2Mn_2O_7$ pyrochlores (A = Y, In, Lu, and Tl). *Phys. Rev. B.* **59**, 1249 (1999).
62. Singh, D. J. Magnetoelectronic effects in pyrochlore $Tl_2Mn_2O_7$: role of Tl-O covalency. *Phys. Rev. B.* **55**, 313 (1997).
63. Núñez Regueiro, M. D. & Lacroix, C. Origin and pressure dependence of ferromagnetism in $A_2Mn_2O_7$ pyrochlores (a = Y, in, lu, and tl). *Phys. Rev. B.* **63**, 014417 (2000).
64. Hamberg, I. & Granqvist, C. G. Evaporated sn-doped In_2O_3 films: Basic optical properties and applications to energy-efficient windows. *J. Appl. Phys.* **60**, R123 (1986).
65. Bhachu, D. S. et al. Origin of high mobility in Molybdenum-dopedIndium oxide. *Chem. Mater.* **27**, 2788 (2015).
66. Söllinger, W. et al. Exchange interactions in europium monochalcogenide magnetic semiconductors and their dependence on hydrostatic strain. *Phys. Rev. B.* **81**, 155213 (2010).
67. Jutong, N., Eckern, U., Mairoser, T. & Schwingenschlögl, U. Effect of Gd doping and O deficiency on the Curie temperature of EuO. *Sci. Rep.* **5**, 8038 (2015).
68. Choi, E.-M., Kleibeuker, J. E. & MacManus-Driscoll, J. L. Strain-tuned enhancement of ferromagnetic T_C to 176 K in Sm-doped $BiMnO_3$ thin films and determination of magnetic phase diagram. *Sci. Rep.* **7**, 43799 (2017).
69. Mairoser, T. et al. Influence of the substrate temperature on the curie temperature and charge carrier density of epitaxial Gd-doped EuO films. *Appl. Phys. Lett.* **98**, 102110 (2011).
70. Melville, A. et al. Lutetium-doped EuO films grown by molecular-beam epitaxy. *Appl. Phys. Lett.* **100**, 222101 (2012).
71. Burg, S., Stukalov, V. & Kogan, E. On the theory of indirect exchange in EuO. *Phys. Status Solidi B.* **249**, 847 (2012).
72. Mairoser, T., Loder, F., Melville, A., Schlom, D. G. & Schmehl, A. Influence of chemical doping on the magnetic properties of EuO. *Phys. Rev. B.* **87**, 014416 (2013).
73. Kresse, G. & Furthmüller, J. Efficiency of ab-initio total energy calculations for metals and semiconductors using a plane-wave basis set. *Comput. Mater. Sci.* **6**, 15 (1996a).
74. Kresse, G. & Furthmüller, J. Efficient iterative schemes for ab initio total-energy calculations using a plane-wave basis set. *Phys. Rev. B.* **54**, 11169 (1996b).
75. Blöchl, P. E. Projector augmented-wave method. *Phys. Rev. B.* **50**, 17953 (1994).
76. Kresse, G. & Joubert, D. From ultra soft pseudopotentials to the projector augmented-wave method. *Phys. Rev. B.* **59**, 1758 (1999).
77. Ong, S. P. et al. Python Materials Genomics (pymatgen): a robust, open-source python library for materials analysis. *Comput. Mater. Sci.* **68**, 314 (2013).
78. Wang, L., Maxisch, T. & Ceder, G. Oxidation energies of transition metal oxides within the GGA + U framework. *Phys. Rev. B.* **73**, 195107 (2006).
79. Gonze, X. et al. ABINIT: first-principles approach to material and nanosystem properties. *Comput. Phys. Commun.* **180**, 2582 (2009).
80. Gonze, X. et al. Recent developments in the ABINIT software package. *Comput. Phys. Commun.* **205**, 106 (2016).
81. Hamann, D. R. Optimized norm-conserving Vanderbilt pseudopotentials. *Phys. Rev. B.* **88**, 085117 (2013).
82. van Setten, M. et al. The Pseudo Dojo: training and grading a 85 element optimized norm-conserving pseudopotential table. *Comput. Phys. Commun.* **226**, 39 (2018).
83. Sharma, S., Dewhurst, J. K., Sanna, A. & Gross, E. K. U. Bootstrap approximation for the exchange-correlation kernel of time-dependent density-functional theory. *Phys. Rev. Lett.* **107**, 186401 (2011).
84. Lebègue, S., Arnaud, B., Alouani, M. & Bloechl, P. E. Implementation of an all-electron *GW* approximation based on the projector augmented wave method without plasmon pole approximation: application to Si, SiC, AlAs, InAs, NaH, and KH. *Phys. Rev. B.* **67**, 155208 (2003).
85. Madsen, G. K. & Singh, D. J. BoltzTraP. A code for calculating band-structure dependent quantities. *Comput. Phys. Commun.* **175**, 67 (2006).
86. Hautier, G., Miglio, A., Ceder, G., Rignanese, G.-M. & Gonze, X. Identification and design principles of low hole effective mass p-type transparent conducting oxides. *Nat. Commun.* **4**, 2292 (2013).
87. Verwey, E. J. W. & Heilmann, E. L. Physical properties and cation arrangement of oxides with spinel structures I. Cation arrangement in spinels. *J. Chem. Phys.* **15**, 174 (1947).
88. Grimes, N. W. & Isaac, E. D. A simplified interpretation of the magnetic exchange interactions for chromium chalcogenide spinels. *Philos. Mag.* **35**, 503 (1977).
89. Rudolf, T. et al. Optical properties of $ZnCr_2Se_4$. *Eur. Phys. J. B.* **68**, 153 (2009).
90. Greedan, J., Raju, N. & Subramanian, M. Structure and magnetic properties of the pyrochlore $Sc_2Mn_2O_7$. *Solid State Commun.* **99**, 399 (1996).
91. Knoke, G. T., Niazi, A., Hill, J. M. & Johnston, D. C. Synthesis, structure, and ferromagnetism of the oxygen defect pyrochlore system $Lu_2V_2O_{7-x}$ (x = 0.40–0.65). *Phys. Rev. B* **76**, 054439 (2007).
92. Chiba, H., Atou, T. & Syono, Y. Magnetic and electrical properties of$Bi_{1-x}Sr_xMnO_3$: hole-doping effect on ferromagnetic perovskite $BiMnO_3$. *J. Solid State Chem.* **132**, 139 (1997).
93. Dass, R. I., Yan, J.-Q. & Goodenough, J. B. Oxygen stoichiometry, ferromagnetism, and transport properties of $La_{2-x}NiMnO_{6+\delta}$. *Phys. Rev. B.* **68**, 064415 (2003).
94. Dass, R. I. & Goodenough, J. B. Multiple magnetic phases of $La_2CoMnO_{6-\delta}$ ($0 \le \delta \le 0.05$). *Phys. Rev. B.* **67**, 014401 (2003).
95. Azuma, M. et al. Designed ferromagnetic, ferroelectric Bi_2NiMnO_6. *J. Am. Chem. Soc.* **127**, 8889 (2005).
96. Takata, K., Azuma, M., Shimakawa, Y. & Takano, M. New ferroelectric ferromagnetic bismuth double-perovskites synthesized by high-pressure technique. *J. Jpn. Soc. Powder Powder Metall.* **52**, 913 (2005).